Nuclear Instruments and Methods in Physics Research B 118 (1996) 663–669

ELSEVIER

NIM B
Beam Interactions with Materials & Atoms

Application of ion-beam-analysis techniques to the study of irradiation damage in zirconium alloys

L.M. Howe [a,*], D. Phillips [a], H. Zou [a], J. Forster [a], R. Siegele [b], J.A. Davies [b], A.T. Motta [c], J.A. Faldowski [c], P.R. Okamoto [d]

[a] *AECL Research, Chalk River Laboratories, Chalk River, Ontario, Canada, K0J 1J0*
[b] *Accelerator Laboratory, McMaster University, Hamilton, Ontario, Canada, L8S 4M1*
[c] *Department of Nuclear Engineering, Pennsylvania State University, University Park, PA 16802, USA*
[d] *Materials Science Division, Argonne National Laboratory, Argonne, IL 60439, USA*

Abstract

Ion-beam-analysis techniques are being used to provide an understanding of the nature of collision cascades, irradiation-induced phase changes, lattice location of solute atoms and defect-solute atom interactions in various zirconium alloys. In zirconium intermetallic compounds, such as Zr_3Fe, Zr_2Fe, $ZrFe_2$, and $Zr_3(Fe_x,Ni_{1-x})$, electron and ion irradiations have been used to obtain detailed information on the crystalline-to-amorphous transformation occurring during the irradiation. Transmission-electron-microscopy (TEM) observations have provided information on the nature of the damage produced in individual cascades, the critical dose required for amorphization, and the critical temperature for amorphization. In a study on the electron-energy dependence of amorphization in Zr_3Fe, Zr_2Fe and $ZrCr_2$ in situ high-voltage-electron-microscope investigations were combined with high-energy forward-elastic-recoil measurements to yield information on the threshold displacement energies for Zr and Fe or Cr in these lattices, as well as the role of secondary displacements of lattice atoms by recoil impurities (C,O) at low electron energies. In Zr implanted with ^{56}Fe ions and subsequently bombarded with ^{40}Ar ions at 723 K, subsequent secondary-ion-mass-spectrometry (SIMS) analyses were used to monitor the effect of irradiation on the migration of Fe in the Zr lattice. In addition, ion-channeling investigations have been used to determine the lattice sites of solute atoms in Zr as well as the details of the interaction between the solute atoms and the irradiation-produced defects.

1. Introduction

Ion-beam-analysis techniques are well suited to provide information on various irradiation effects that occur in zirconium alloys during irradiation. These effects include irradiation-induced phase changes, irradiation-enhanced precipitation and defect–solute atom interactions. The above effects may play a significant role in affecting the deformation and corrosion behaviour of zirconium alloys in either calandria or pressure tubes in CANDU nuclear reactors. The behaviour of zirconium intermetallic compounds containing Fe, Cr, Ni or Nb is of particular interest since an irradiation-induced crystalline-to-amorphous transformation has been observed for $Zr(Cr,Fe)_2$ and $Zr_2(Ni,Fe)$ precipitates in Zircaloy-2 and Zircaloy-4; see Refs. [1–4] for example. Zr–Nb–Fe precipitates may also be present in Zr–2.5Nb alloys used in pressure tubes in CANDU reactors. In addition, Fe controls self and substitutional diffusion in both α-Zr and the α-based zirconium alloys Zircaloy-2, Zircaloy-4 and Zr–2.5Nb [5,6]. Fe also appears to play an important role in affecting the in-reactor deformation behaviour of Zircaloy-2 and Zr–2.5Nb [7,8].

In the present paper the principal results of investigations of collision cascades and irradiation-induced amorphization of various zirconium intermetallic compounds during ion and electron irradiation will be summarized. Results will also be presented for determining the threshold displacement energies for the constituent atoms (including light element impurities) in Zr_3Fe, Zr_2Fe and $ZrCr_2$, as obtained from studies of the electron-energy dependence of amorphization in these intermetallic compounds, along with a determination of the concentration of the light element impurities from forward elastic-recoil measurements using 230 MeV ^{209}Bi ions. An ion implantation and subsequent irradiation procedure, followed by a SIMS analysis has provided information on the trapping of migrating Fe atoms in Zr by irradiation-produced defects. The results of studies of ion-channeling investigations on the location of the lattice positions of Au and N atoms in Zr and the interaction between these solute atoms and the irradiation-produced defects will also be presented.

* Corresponding author, tel. 613 584 3311, fax 611 584 3250, e-mail: howe@crf.accl.ca.

SSDI 0168-583X(95)01171-40

2. Experimental details

The bulk phases of Zr_3Fe, (orthorhombic), $Zr_3(Fe_xNi_{1-x})$ (orthorhombic), Zr_2Fe (tetragonal), $ZrFe_2$ (cubic Laves phase), and $ZrCr_2$ (cubic Laves phase) were obtained by the appropriate heat treatments from arc melted alloys. Samples suitable for transmission-electron-microscopy (TEM), forward-elastic-recoil detection, ion channeling or secondary-ion-mass spectrometry (SIMS) were obtained by a combination of spark cutting, mechanical polishing, and finally either chemical or electropolishing procedures.

The heavy-ion bombardments were performed at Chalk River Laboratories (CRL) using one of the following: a 70 kV ion implanter, a high-voltage mass separator or a 2.5 MV Van de Graaff. Ion channeling investigations were performed using a 2.5 MV Van de Graaff accelerator at CRL. Forward-elastic-recoil measurements were performed using 230 MeV ^{209}Bi ions produced by the Tandem accelerator in the TASCC facility at CRL. The recoiling target atoms were detected in a specially designed ΔE–E detector [9]. The in situ electron bombardments were performed on the Kratos high-voltage electron microscope (HVEM) at Argonne National Laboratory. The SIMS analysis was performed using a CAMECA 4F at CANMET. Detailed electron-microscope observations (TEM) and EDX analyses were performed using a Philips CM30 electron microscope at CRL.

3. Results and discussion

3.1. Collision cascades and irradiation-induced amorphization in zirconium intermetallic compounds

A detailed TEM study has been performed of the damage produced in individual collision cascades by 15–350 keV ^{209}Bi ion bombardments of Zr_3Fe, Zr_2Fe and $ZrFe_2$ [10,11]. Examples of the damage visible in the TEM are shown in Fig. 1. The majority of the damaged regions had diameters in the range 1.0 to 5.0 nm.

At high values for the average deposited-energy density $\bar{\theta}_v$ in the cascade, which corresponded to low energy heavy-ion implants (e.g. 15–30 keV Bi in Zr_3Fe, Zr_2Fe and $ZrFe_2$) the visible damage produced in a cascade consisted of a single damaged region, as shown in Fig. 1a. $\bar{\theta}_v$ is a measure of the average amount of energy expended in nuclear collision events, that is deposited per atom in the volume occupied by an individual collision cascade [10,11]. With decreasing values of $\bar{\theta}_v$ (i.e. increasing ion implant energies), there was an increasing tendency for multiple damaged regions (subcascades) to form within a main cascade, as shown in Fig. 1b. The visible damaged regions appeared to be amorphous. It was also found that as the Bi ion energy increased ($\bar{\theta}_v$ decreased), the fraction F of the theoretical collision cascade volume that was occupied by the visible damaged regions within a cascade decreased rapidly. The theoretical collision-cascade volume was taken as the volume of the spheroid whose axes were determined by the longitudinal $\langle \Delta X^2 \rangle^{1/2}$ and transverse $\langle Y^2 \rangle^{1/2}$ straggling components of the statistical damage distribution [12,13]. The crystalline-to-amorphous transformation appeared to be the result of direct amorphization within the collision cascades and a critical defect concentration being reached in the cascade overlap regions, thus producing additional amorphous regions.

Detailed information has been obtained for irradiation-induced amorphization of Zr_3Fe, Zr_2Fe $ZrFe_2$, $ZrCr_2$ and $Zr_3(Fe_x,Ni_{1-x})$ alloys during irradiation with heavy ions [10,11,14–16] (i.e. 0.5–1.5 MeV ^{40}Ar ions and 0.015–1.5 MeV ^{209}Bi ions) and with electrons (0.2–0.9 MeV) in a high-voltage electron microscope (HVEM) [17–20]. It was found that the critical temperature (i.e. the temperature above which amorphization does not occur) for amorphization with electrons was always considerably lower than under heavy-ion bombardment. Depending upon the particular intermetallic compound, the critical temperatures for electron irradiation were in the range ~75 to 250 K,

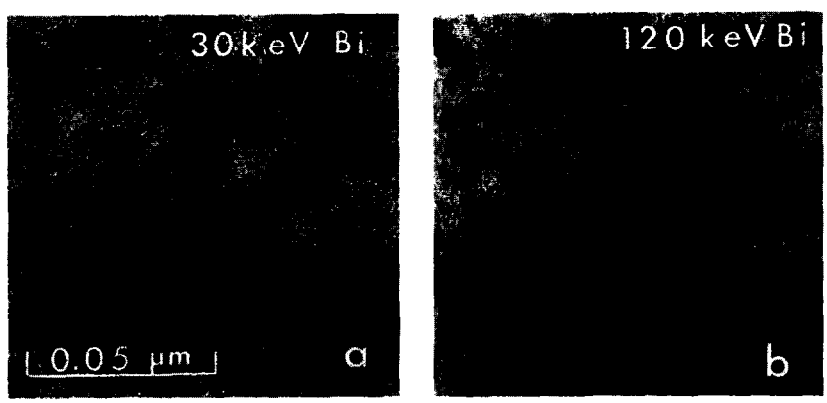

Fig. 1. Bright-field electron micrographs of Zr_3Fe irradiated at 40 K with (a) 30 keV ^{209}Bi ions to a fluence of 2.5×10^{11} ions cm^{-2} and (b) 120 keV ^{209}Bi ions to a fluence of 1.0×10^{11} ions cm^{-2}.

whereas the critical temperatures for heavy-ion irradiation were ~ 500–600 K. Also, in the vicinity of the critical temperature for the electron irradiations there was a significant dose-rate dependence, with the highest critical temperature occurring at the highest dose rate [17]. Appreciable effects of dose rate on the irradiation-induced amorphization were also observed for heavy-ion irradiations in temperature regimes where significant annealing of defects was occurring. In Zr_3Fe, for example, in the temperature range 160–280 K there was a pronounced dose-rate effect for 0.5–1.5 MeV ^{40}Ar ion irradiations. The fraction of the irradiated volume that had been rendered amorphous at a given ^{40}Ar ion fluence increased noticeably as the ion flux was increased from 0.9×10^{11} to 14.7×10^{11} ions $cm^{-2} s^{-1}$ [15]. Near the critical temperature, as the dose rate increases there is less chance for annealing to occur before the next damage event, and thus it is easier to amorphize the material. Also, for the ^{40}Ar and ^{209}Bi ion irradiations of Zr_3Fe, a step occurred in the dose-to-amorphization curve in the same temperature region (~ 180–220 K) as that for the critical temperature for electron irradiation [16]. However, the critical temperature for the amorphization of Zr_3Fe by ^{40}Ar ion irradiation was 570–600 K, and slightly higher (~ 625 K) for ^{209}Bi ion irradiation [16].

In the case of the $ZrFe_2$ and $ZrCr_2$ intermetallic compounds (both having a cubic Laves structure), the morphology of the alloys was such that there were two distinct regions of the same $ZrFe_2$ or $ZrCr_2$ phases; one of which contained a high density of stacking faults and the other containing a low density of stacking faults. For both $ZrFe_2$ and $ZrCr_2$, the critical temperatures for electron irradiation were higher for the regions containing the high density stacking faults than they were for the low density stacking fault regions; a difference of ~ 20 K for $ZrFe_2$ and ~ 10 K for $ZrCr_2$ [20]. Also, in $ZrFe_2$ the electron dose required for amorphization to occur at the lowest irradiation temperatures (25–35 K) was ~ 2 times lower for the high density stacking-fault regions than it was for the low density stacking-fault regions. Regions containing stacking faults are high-energy regions and the local distortion of the lattice or high chemical energy gives an additional contribution to the free energy rise resulting from irradiation, thus facilitating the crystalline-to-amorphous transformation. Also, there could be a change in defect mobility or possibly a change in diffusion modes caused by the presence of the stacking faults.

The results of the ion and electron irradiations can be understood in the framework of damage accumulation under irradiation. Damage produced by irradiation is opposed by thermal annealing. The balance between the rate of damage production and the ability of the material to repair itself dictates the response of the material to irradiation. At low temperatures, damage produced by irradiation remains "frozen in", with little annealing taking place. In this temperature regime, the dose-to-amorphization is almost independent of the temperature: the damage accumulates in the lattice, unchecked by thermal annealing. At a certain level of irradiation damage, there appears to be a driving force to exchange the imperfect form of long-range order resulting from irradiation for a local configuration of short-range order, where the bonding restrictions of chemical species and directionality are followed more closely. The difference between the ion and electron irradiations results from the fact that ion irradiation produces displacement cascades, while electron irradiation produces isolated Frenkel pairs. Within the cascades, the density of damage is quite high and amorphization can then occur either directly in the cascade or upon cascade overlap. As the irradiation temperature increases, annealing processes are activated that offset the production of damage. When annealing reduces the effective damage rate without overwhelming it, a "step" appears in the dose-to-amorphization vs. temperature curve, increasing the dose-to-amorphization at that temperature. The temperature at which the activated annealing process completely overwhelms damage production is the critical temperature, and amorphization is no longer possible above that temperature. It follows then that a lower damage rate is offset at a lower temperature than at a higher damage rate. This implies different critical temperatures for different damage rates.

3.2. Electron-energy dependence of amorphization in Zr_3Fe, Zr_2Fe and $ZrCr_2$, and the determination of the threshold displacement energies for the atoms in these compounds

Studies were also undertaken to determine the energy dependence of the dose-to-amorphization during electron irradiation of Zr_3Fe, Zr_2Fe and $ZrCr_2$ at 23–30 K [18–20]. Samples from these alloys were irradiated in the HVEM at ANL at energies from 200 to 900 keV. The irradiations were performed at very low temperatures (23–30 K) in order to eliminate any dose-rate effects on the dose-to-amorphization. Amorphization occurred in these alloys at energies from 900 down to ~ 300 keV. The results for the three alloys are shown in Fig. 2. Three distinct regions can be observed in Fig. 2. Between 900 and ~ 700 keV amorphization occurred at the lowest dose, which was relatively constant. A higher plateau of dose-to-amorphization was then present; at 500–600 K for Zr_3Fe, 400–500 K for Zr_2Fe and 550–600 K for $ZrCr_2$. Finally, there was a sharp increase in the dose-to-amorphization below the plateau regions.

The results of the energy dependence experiments can be analyzed in terms of a composite displacement cross section dominated at high energies (~ 700–900 keV) by displacements of Zr and Fe (or Cr) atoms, by displacements of Fe (or Cr) at intermediate energies (~ 400–600 keV) and by secondary displacements of lattice atoms by recoil impurities at low energies (below 400 keV).

To obtain information on the concentration of the light

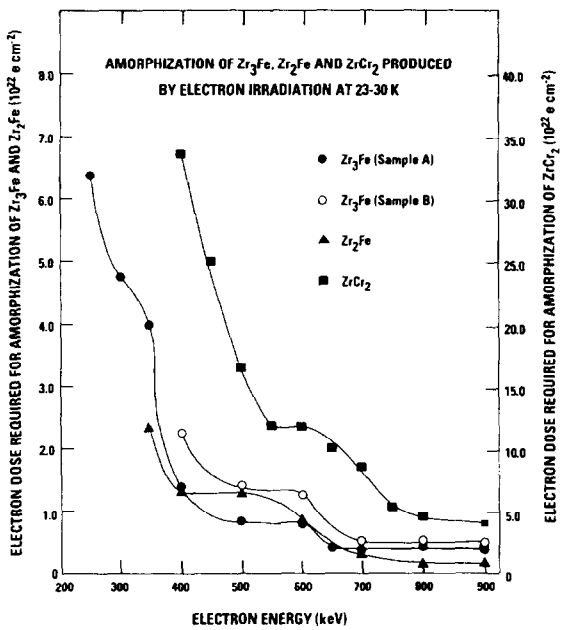

Fig. 2. Dose-to-amorphization for Zr_3Fe (for two different samples), Zr_2Fe and $ZrCr_2$ at 23–30 K as a function of the incident electron energy.

element impurities present in the samples, forward-elastic-recoil measurements using 230 MeV ^{209}Bi ions were performed. The recoiling target atoms were detected in a specially designed ΔE–E detector [9]. This technique also enabled us to determine the depth distribution of the light element impurities over a depth that was comparable to that used for HVEM examinations (i.e. ~200–350 nm), or up to ~1000 nm for the 0.5–1.5 MeV ^{40}Ar ion irradiations.

A typical example of a coincidence ΔE–E spectra is shown in Fig. 3 for one of the zirconium intermetallic compounds. It can be seen that the principal light element impurities are O and C. The results, for the various alloys used in the present investigations, indicate that near the surface region ($< \sim 25$ nm), the O and C levels are ~4–10 atom % and ~1–3 atom % respectively. Below this surface region in the bulk of the specimen the O and C levels range from ~0.5–2.0 atom % and ~0.25–1.0 atom %, respectively.

For these low temperature electron irradiations performed on Zr_3Fe, Zr_2Fe and $ZrCr_2$, annealing of the irradiation-produced defects is not a factor, and therefore there is no dose rate effect, as observed experimentally. Amorphization occurs when the dose-to-amorphization is equal to the critical dose D_{crit}, i.e. at a constant dpa, which is specific for each intermetallic compound. Consequently, for each electron energy E at amorphization:

$$D(E) = \phi t_{am}(E)\sigma_d(E) = \phi t_{am}(E)\sum_i x_i \sigma_d^i\left(E_d^i, E\right) = D_{crit}, \quad (1)$$

where $D(E)$ is the dose-to-amorphization, ϕ is the electron flux, t is the measured time-to-amorphization, x_i is the concentration of element i, σ_d^i (E_d^i, E) is the displacement cross section, E_d^i is the displacement threshold energy and D_{crit} is the critical dose for amorphization. Eq. (1) states that when we multiply the values of the dose-to-amorphization as a function of energy (as given in Fig. 2, for example), by the weighted displacement cross section (obtained from the tabulations by Oen [21]), the result should be independent of energy. Since the values from Oen's tables [21] are dependent on the displacement energy, it is possible to find the set of displacement energies that best fits the experimental data.

As mentioned above, displacements can also occur by a secondary displacement mechanism, mediated by light element impurities. The forward-elastic-recoil measurements show that O is the major light element impurity in the zirconium intermetallic compounds used in this investigation. Hence, if the displacements produced by a secondary displacement mechanism are also taken into account, then:

$$D(E) = \phi t_{am}(E)\left[x_{Zr}\sigma_d^{Zr}\left(E_d^{Zr}, E\right) + x_{Fe(Cr)}\sigma_d^{Fe(Cr)}\left(E_d^{Fe(Cr)}, E\right) + x_O\sigma_d^O\left(E_d^O, E\right)\vartheta_O^{Zr,Fe(Cr)}\right] = D_{crit}, \quad (2)$$

where $\vartheta_O^{Zr,Fe(Cr)}$ is the number of displacements in the Zr,Fe(Cr) lattices caused by each O displacement. ($\vartheta_O^{Zr,Fe(Cr)}$ was taken to be 1).

Using the appropriate values of x_{Zr} and $x_{Fe(Cr)}$ for each of the major alloying elements (i.e. Zr, Fe or Cr), as well as the value of x_O for the light element impurity O, the displacement threshold energies can be obtained. The specific x_O values used for Zr_3Fe (sample A), Zr_3Fe (sample B), Zr_2Fe and $ZrCr_2$ were 0.03, 0.01, 0.02 and

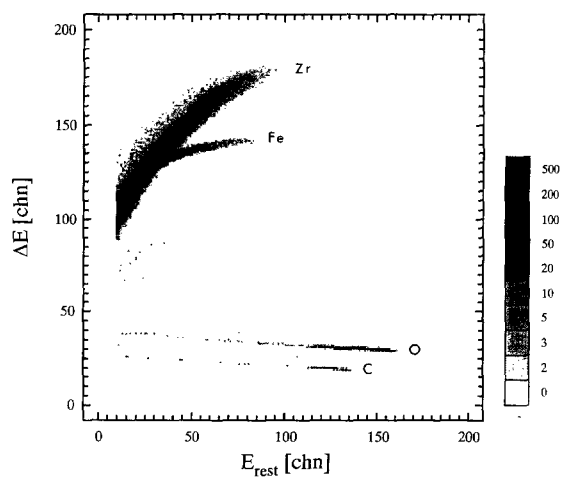

Fig. 3. Coincidence ΔE–E spectrum of a Zr–25.0 at.% Fe alloy obtained using a 230 MeV ^{209}Bi ion beam.

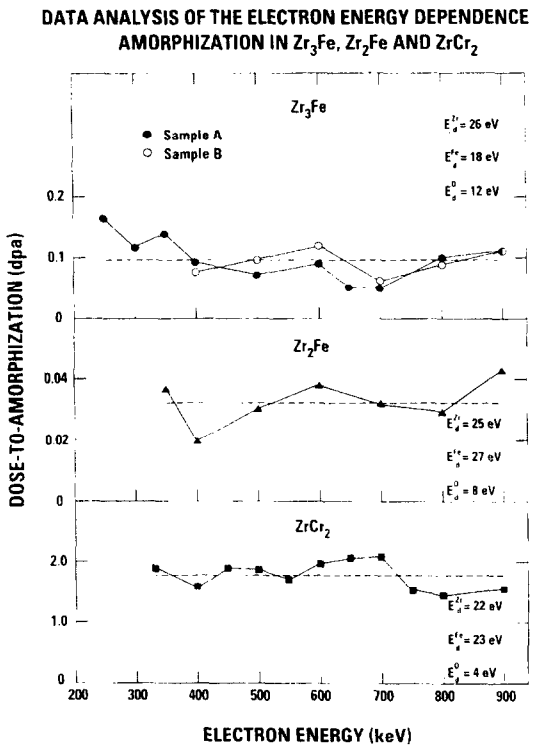

Fig. 4. The optimized profile for dose-to-amorphization (in dpa) versus electron energy for Zr_3Fe (for two samples having different O concentrations), Zr_2Fe and $ZrCr_2$. The dotted horizontal lines represent the average of the D (dose-to-amorphization) values for each set of data.

0.025, respectively. Eq. (2) was used to fit the data by minimizing the least squares deviation from the horizontal. The results of the analysis are shown in Fig. 4.

The specific values obtained for the displacement threshold energies were as follows:

1) Zr_3Fe (an orthorhombic phase): $E_d^{Zr} = 26$ eV, $E_d^{Fe} = 18$ eV and $E_d^O = 12$ eV.
2) Zr_2Fe (a tetragonal phase): $E_d^{Zr} = 25$ eV, $E_d^{Fe} = 27$ eV and $E_d^O = 8$ eV.
3) $ZrCr_2$ (a cubic Laves phase): $E_d^{Zr} = 22$ eV, $E_d^{Cr} = 23$ eV and $E_d^O = 4$ eV.

Hence from a detailed analysis of the electron energy dependence of amorphization of Zr_3Fe, Zr_2Fe and $ZrCr_2$ it has been possible to obtain the specific values for the displacement threshold energies for the atoms on the sublattices in these compounds, as well as to assess the importance of secondary displacement events produced by light element impurities.

3.3. Trapping of Fe by irradiation-produced defects in Zr

In order to investigate the effect of irradiation on the trapping of Fe by irradiation-produced defects in Zr, ion implantations have been combined with a SIMS analysis of the implanted Fe depth profile. Initially two Zr single crystals were implanted at 35 K with 1.0 MeV ^{56}Fe ions to a fluence of 2.5×10^{15} ions cm^{-2}. Subsequent ion implantations of the two crystals were performed at 723 K with 0.9 MeV ^{40}Ar ions to fluences of either 5.0×10^{14} or 5.0×10^{15} ^{40}Ar ions cm^{-2}. During the ^{40}Ar ion bombardment, one-half of each crystal was masked to serve as an unirradiated reference where only thermal annealing occurred. The energy of the ^{40}Ar ion beam (i.e. 0.9 MeV) was chosen so that the damage distribution produced by the ^{40}Ar ions was similar to the range profile of the implanted 1.0 MeV ^{56}Fe ions.

The results are shown in Figs. 5 and 6. In the absence of the ^{40}Ar ion irradiation at 723 K, appreciable migration

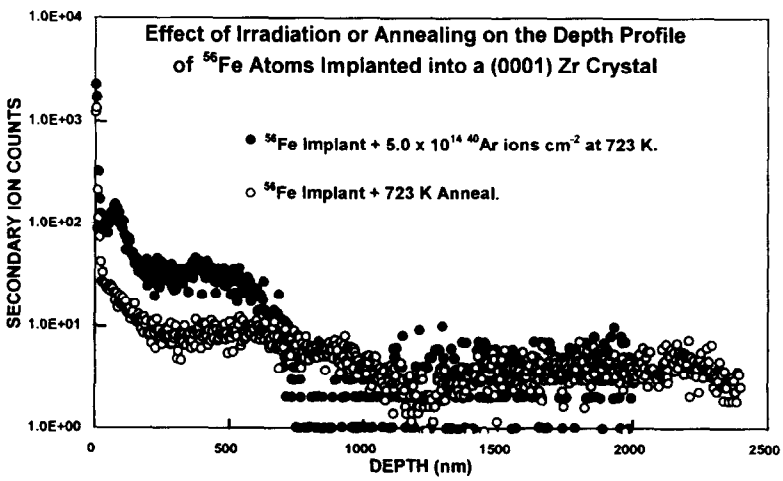

Fig. 5. Effect of irradiation or annealing on the depth profile of ^{56}Fe atoms implanted into a (0001) crystal. The ^{40}Ar ion fluence at 723 K was 5.0×10^{14} ions cm^{-2}.

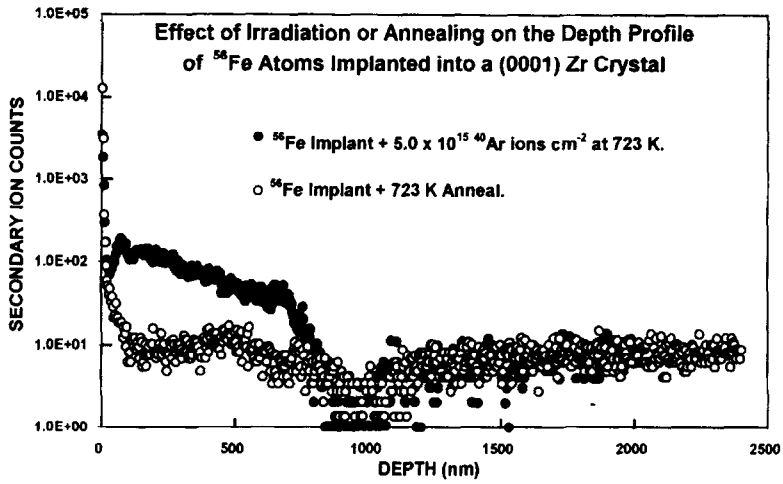

Fig. 6. Effect of irradiation or annealing on the depth profile of ^{56}Fe atoms implanted into a (0001) crystal. The ^{40}Ar ion fluence at 723 K was 5.0×10^{15} ions cm^{-2}.

of the Fe atoms has occurred (see points labelled ^{56}Fe implant + 723 K anneal). This is consistent with various diffusion results which indicate that Fe is a very fast diffusing species in Zr [5,6]. In the presence of the irradiation damage produced by the ^{40}Ar ions at 723 K, the Fe atoms become trapped by the irradiation-produced defects. Consistent with this interpretation, is the fact that the trapping effect is noticeably larger for the higher fluence of ^{40}Ar ions.

Zou et al. [22] have combined ion implantation and electron microprobe analysis to study irradiation effects on Fe distributions in Zircaloy-2 and Zr–2.5Nb. They irradiated large-grained (10–40 μm) Zircaloy-2 and Zr–2.5Nb specimens with 1.5 MeV ^{40}Ar ions to fluences of $\sim 10^{16}$ ions cm^{-2} at 323, 573 and 693 K. Subsequent electron microprobe analyses revealed that the ^{40}Ar ion irradiations lead to enhanced dissolution of Fe in the α-phase. After irradiation, the α-phase Fe levels were 0.025–0.15 at.% compared to equivalent values of ~ 0.0070 at.% in the non-irradiated state. In Zr–2.5Nb the β-phase Fe levels fell from about 0.60 to 0.35 at.%. Zou et al. [22] propose that the irradiation-driven dissolution of Fe into the α-phase of Zircaloy-2 and Zr–2.5Nb can be understood in terms of irradiation-induced defects and Fe–defect interactions.

3.4. Location of the lattice positions of Au and N atoms in Zr and the interaction between these solute atoms and the irradiation-produced defects

Backscattering of 2.0 MeV ^{4}He ions from Zr–0.2 at.% Au and Zr–0.3 at.% Au crystals were measured for [0001], $\langle 11\bar{2}0\rangle$ and $\langle 10\bar{1}0\rangle$ directions and the (0001) plane in order to determine the trapping characteristics of Au atoms for irradiation-induced defects [23]. It was observed that the Au atoms, which were initially on substitutional sites, formed strong traps for Zr self-interstitial atoms, which became mobile at ~ 120 K. The direction of the Au atom displacements in the trapped configuration was between the $\langle 40\bar{4}3\rangle$ and $\langle 10\bar{1}0\rangle$ axes. The displacement of the Au was reduced during annealing from 200–400 K, and was reduced further from 550–700 K. The recovery stage at 550–700 K is likely due to vacancies. It was initially proposed that the recovery stage at 200–400 K may be due to another type of Zr self-interstitial atom. However, it is now believed that interstitial Fe–vacancy (Fe_iV) complexes are very strongly bound (~ 1.4 eV) and also that they have very low migration energies [24,25]. Hence, it is quite possible that the recovery occurring at 200–400 K, may be the result of the migration of a Fe_iV complex (since the Zr crystals will undoubtedly have Fe present as an impurity), or to the migration of a Au_iV complex.

Ion-channeling techniques were also used to determine the lattice sites of N in the α-Zr hexagonal close-packed (hcp) structure and the effect of trapping irradiation-produced defects at the N atoms [26]. A Zr single crystal was implanted along $\langle 11\bar{2}0\rangle$ at 293 K with 300 keV $^{15}N_2$ ions to a fluence of 2.2×10^{15} ions cm^{-2}. The position of ^{15}N atoms in the Zr lattice was studied using measurements of yields of ^{1}H ions (incident energy 800 keV) backscattered from the Zr atoms and the alpha-particle yields from the nuclear reaction $^{15}N(p,\alpha)^{12}C$. Dechanneling of the protons in the Zr crystal provided information on changes in the overall defect concentration during the irradiation and annealing stages.

Information was obtained for the $\langle 11\bar{2}0\rangle$ and $\langle 10\bar{1}0\rangle$ channels. The ^{15}N ion implantation resulted in an appreciably larger yield of α particles when the ^{1}H ion beam was incident along $\langle 11\bar{2}0\rangle$ compared to that found for incidence along $\langle 10\bar{1}0\rangle$. Angular scans through $\langle 11\bar{2}0\rangle$ also indicated an appreciable peaking in the α-particle yield at

the aligned $\langle 11\bar{2}0 \rangle$ position. These observations indicated that the N atoms occupied the octahedral interstitial positions in the α-Zr hcp lattice.

Subsequent to the ^{15}N implantation, the Zr crystal was irradiated at 35 K with 800 keV ^{4}He ions to fluences of 1.8×10^{16} and 9.1×10^{16} ions cm^{-2}, followed by post-irradiation annealing in both instances. No appreciable displacement of the N atoms from their lattice sites was detected after these irradiations, or during annealing up to 423 K. Hence N atoms in octahedral sites are very stable and their position remains essentially unaltered during subsequent defect formation and migration, at least up to 423 K.

4. Conclusions

Ion and electron irradiations, ion implantation and various ion-beam analyses have provided the following information on irradiation damage in zirconium alloys:

1) Detailed information on the nature of the damage produced in individual collision cascades in Zr_3Fe, Zr_2Fe and $ZrFe_2$.
2) An understanding of the mechanisms controlling irradiation-induced amorphization in various zirconium intermetallic compounds.
3) Values of the threshold displacement energies for the constituent atoms (including light element impurities) in Zr_3Fe, Zr_2Fe and $ZrCr_2$.
4) Trapping of migrating Fe atoms in Zr by irradiation-produced defects.
5) Location of the lattice position of Au and N atoms in Zr and the interaction between these solute atoms and the irradiation-produced defects.

Acknowledgements

This research project was funded mainly through a CANDU Owners Group (COG) contract and we wish to thank the COG Working Party 32 committee for their financial support and interest in the program. The authors would also like to express their appreciation for the technical support they received from H. Plattner and J.D. Bonnett of Chalk River Laboratories and from E. Ryan, L. Funk and S. Ackers of Argonne National Laboratory.

References

[1] W.J.S. Yang, R.P. Tucker, B. Cheng and R.B. Adamson, J. Nucl. Mater. 138 (1986) 185.
[2] M. Griffiths, J. Nucl. Mater. 159 (1988) 190.
[3] F. Lefebvre and C. Lemaignan, J. Nucl. Mater. 165 (1989) 122.
[4] A.T. Motta, F. Lefebvre and C. Lemaignan, in: Zirconium in the Nuclear Industry, 9th Int. Symp., Kobe, Japan, 1990, eds. C.M. Euken and A.M. Garde, ASTM, STP 1132 (1991) 718.
[5] G.M. Hood, Defect and Diffusion Forum 95–98 (1994) 755.
[6] T. Laursen, G.M. Hood, R. Belec, G.R. Palmer, R.J. Schultz and J.L. Whitton, Nucl. Instr. and Meth. B 64 (1992) 475.
[7] M. Griffiths, R.W. Gilbert and V. Fidleris, ASTM-STP 1023 (1989) 658.
[8] R.G. Fleck, J.E. Elder, A.R. Causey and R.A. Holt, in: Zirconium in the Nuclear Industry, 10th Int. Symp. Baltimore, MD., June 1993, eds. A.M. Garde and E.R. Bradley, ASTM, STP 1245 (1994) 168.
[9] R. Siegele, H.K. Haugen, J.A. Davies, J.S. Forster and H.R. Andrews, J. Appl. Phys. 76 (8) (1994) 4524.
[10] L.M. Howe, M.H. Rainville, D. Phillips, H. Plattner and J.D. Bonnett, Nucl. Instr. and Meth. B 80/81 (1993) 73.
[11] L.M. Howe, D. Phillips, H.H. Plattner and J.D. Bonnett, Nucl. Instr. and Meth. B 102 (1995) 77.
[12] K.B. Winterbon, P. Sigmund and J.B. Sanders, K. Dan, Vidensk. Selsk. Mat. Fys. Medd. 37 (1970) 14.
[13] K.B. Winterbon, Ion Implantation Range and Energy Deposition Distributions, vol. 2 (Plenum, New York, 1975).
[14] L.M. Howe, D.P. McCooeye, M.H. Rainville, J.D. Bonnett and D. Phillips, Nucl. Instr. and Meth. B 59/60 (1991) 884.
[15] L.M. Howe, M.H. Rainville and D. Phillips, in: Phase Formation and Modification by Beam–Solid Interactions, eds. G.S. Was, L.E. Rehn and D.M. Follstaedt, Mater. Res. Soc. Symp. Proc. 235 (1992) p. 461.
[16] L.M. Howe, D. Phillips, A.T. Motta and P.R. Okamoto, Surf. and Coatings Technol. 66 (1994) 411.
[17] A.T. Motta, L.M. Howe and P.R. Okamoto, J. Nucl. Mater. 205 (1993) 258.
[18] A.T. Motta, L.M. Howe and P.R. Okamoto, in: Materials Synthesis and Processing Using Ion Beams, eds. R.J. Cutlbertson, O.W. Holland, K.S. Jones and K. Maex, Mater. Res. Soc. Symp. Proc. 316 (1994) 265.
[19] A.T. Motta, L.M. Howe and P.R. Okamoto, in: Microstructure of Irradiated Materials, eds. I.M. Robertson, L.E. Rehn, S.J. Zinkle and W.J. Phythian, Mater. Res. Soc. Symp. Proc. 373 (1995) 183.
[20] J.A. Faldowski, A.T. Motta, L.M. Howe and P.R. Okamoto, submitted for publication in Symp. on Thermodynamics and Kinetics of Phase Transformation, 1995 Fall Meeting MRS, Nov. 27–Dec. 1, 1995; also in Appl. Phys. Lett. (1995).
[21] O.S. Oen, ORNL report 4897 (1973).
[22] H. Zou, G.M. Hood, J.A. Roy and R.H. Packwood, in: Microstructure of Irradiated Materials, eds. I.M. Robertson, L.E. Rehn, S.J. Zinkle and W.J. Phythian, Mater. Res. Soc. Symp. Proc. 373 (1995) 201.
[23] M.L. Swanson, L.M. Howe, A.F. Quenneville and J.F. Watters, J. Nucl. Mater. 67 (1977) 42.
[24] M. Eldrup, G.M. Hood, N.J. Pederson and R.J. Schultz, Mater. Sci. Forum 105–110 (1992) 997.
[25] A.D. King, G.M. Hood and R.A. Holt, J. Nucl. Mater. 185 (1991) 174.
[26] L.M. Howe and M.L. Swanson, Nucl. Instr. and Meth. B 64 (1992) 246.